Association in Aqueous Solutions of a Thermoresponsive PVCL-*g*-$C_{11}EO_{42}$ Copolymer

Anna-Lena Kjøniksen,[†] Antti Laukkanen,[‡] Céline Galant,[§] Kenneth D. Knudsen,[§] Heikki Tenhu,[‡] and Bo Nyström*,[†]

Department of Chemistry, University of Oslo, P.O. Box 1033, Blindern, N-0315 Oslo, Norway; Laboratory of Polymer Chemistry, University of Helsinki, PB 55, FIN-00014 Helsinki, Finland; and Department of Physics, Institute for Energy Technology, P.O. Box 40, N-2027 Kjeller, Norway

Received July 14, 2004; Revised Manuscript Received November 11, 2004

ABSTRACT: Thermoresponsive associations in aqueous solution of poly(*N*-vinylcaprolactam) chains grafted with *ω*-methoxy poly(ethylene oxide) undecyl α-methacrylate (PVCL-*g*-$C_{11}EO_{42}$) at different copolymer concentrations have been investigated with the aid of various experimental methods. Turbidity measurements reveal that the cloud point (CP) decreases with increasing polymer concentration, and this effect is more pronounced in the semidilute concentration regime. Small-angle neutron scattering (SANS) results at large scattering wavevectors suggest a gradual conformational transition from random coils to contracted coils in the dilute concentration regime as the temperature rises. The rheological experiments disclose a strong temperature-induced contraction of the molecules in the dilute concentration regime, and the results in the semidilute regime indicate that the polymer chains are unentangled even at high concentrations. Dynamic light scattering results on solutions at temperatures up to the CP show the existence of a bimodal relaxation process; one mode is associated with the diffusion of individual polymer coils, or small clusters of molecules, and the other one is ascribed to interchain aggregation and the formation of aggregates at higher concentrations. At low concentrations, the intrachain species exhibit a temperature-induced compression, whereas at higher concentrations a temperature rise generates intermolecular aggregates. At a low constant temperature, an increase in polymer concentration leads to poorer thermodynamic conditions of the system, and shrinkage of the polymer coils is observed. At temperatures slightly above CP, the decay of the correlation function is characterized by a narrow unimodal relaxation mode. At this stage, most of the intrachain structures have been consumed in the formation of more compact particles.

Introduction

In recent years, thermally responsive block and graft amphiphilic copolymers have attracted extensive attention both for their intrinsic scientific interest and for their technological importance.[1−14] Some of these macromolecules are attractive as biomaterials in applications such as drug delivery, tissue engineering, and other biomedical devices.[15−20] In aqueous solution, the introduction of hydrophilic/amphiphilic grafts of the polymer may promote the buildup of core−shell-like nanoparticles, consisting of a hydrophobic core surrounded by a hydrophilic shell. An aqueous solution of this type of polymer is characterized by a phase separation upon heating, and the system exhibits a lower critical solution temperature (LCST).[21−23] At low temperature the solution is homogeneous, but when the temperature exceeds a critical value called the cloud point (CP) of the mixture, a macroscopic phase separation appears. The LCST corresponds to the minimum of the phase separation curve.[24,25]

The temperature responsive polymer poly(*N*-vinylcaprolactam) (PVCL) belongs to the above-mentioned category of polymers that recently has attracted a great deal of interest.[14,20,26−30] This polymer is stable against hydrolysis, nonionic, and biocompatible,[19] and it has a LCST near body temperature. These properties make it an interesting candidate for biomedical applications.[31] However, in connection with the collapse of the individual polymer particles, it is well-known that also interparticle aggregation can take place. The latter process constitutes a serious complication in many practical applications. The tendency of the polymer to associate can be reduced or eliminated by making the particle surface charged or sterically stabilized.[32] Poly(ethylene oxide) (PEO) is a hydrophilic biocompatible polymer that is known[33] to be an effective stabilizing agent. The synthetic strategy is to produce PVCL that is grafted with PEO. Alternatively, reactive PEO methacrylates have also been used[34,35] as macromonomers.

In the present work an amphiphilic macromonomer ($MAC_{11}EO_{42}$) has been synthesized that is composed of a PEO segment (42 ethylene oxide units) and a relatively short hydrophobic alkyl chain (11 methylene units), and a reactive methacrylate is incorporated[27] at the hydrophobic end of the molecule. The reaction between this macromonomer and VCL yields the grafted copolymer poly(*N*-vinylcaprolactam)-*graft*-*ω*-methoxy poly(ethylene oxide) undecyl α-methacrylate,[36] which henceforth will be referred to as PVCL-*g*-$C_{11}EO_{42}$. This thermoresponsive copolymer is easily soluble in water at ambient temperature but exhibits a LCST at elevated temperature. The PVCL segments mainly give rise to the hydrophobic feature of the copolymer, whereas the ethylene oxide moieties provide the polymer with its hydrophilic character. The chemical structures of VCL, the amphiphilic macromonomer, and the grafted copolymer are all depicted in Figure 1.

To gain insight into the complex interplay between intrachain and interchain aggregation in aqueous solutions of the grafted amphiphilic copolymer PVCL-*g*-C_{11}-

[†] University of Oslo.
[‡] University of Helsinki.
[§] Institute for Energy Technology.

10.1021/ma048581q CCC: $30.25
Published on Web 01/11/2005

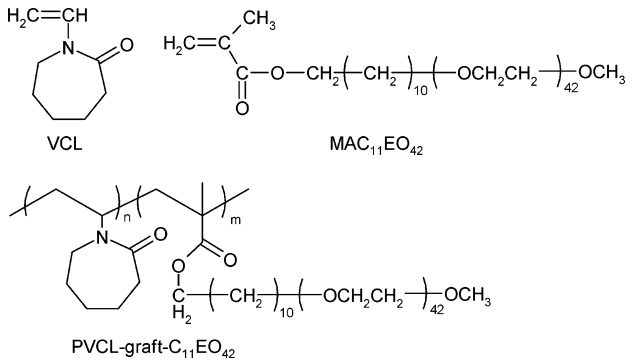

Figure 1. Chemical structures of the components and the grafted copolymer.

EO_{42}, we have carried out turbidity, small-angle neutron scattering (SANS), rheological, and dynamic light scattering (DLS) measurements over an extended polymer concentration range and over a broad temperature interval. The intention with the range of experimental techniques is to provide detailed information about thermodynamic, structural, rheological, and dynamical features in these polymer solutions under various conditions. The objective is to obtain a detailed picture of the competition between intrachain behavior and interchain association in the process of understanding self-assembling of amphiphilic copolymers. In a forthcoming publication, the effect of addition of an ionic surfactant on the association behavior will be addressed.

Experimental Section

Materials. *N*-Vinylcaprolactam (VCL, 98%) was obtained from Aldrich Chemicals, Germany, and was purified by recrystallization from benzene. 2,2'-Azobis(isobutyronitrile) (AIBN, Aldrich Chemicals, Switzerland) was purified by recrystallization from methanol. Tetrahydrofuran (THF) and hexane (both HPLC grade from Rathburn, Scotland) and benzene (99.7%, Reidel-de-Haen, Germany) were all used without further purification.

Polymerization and Solutions Preparations. The amphiphilic PEO macromonomer $MAC_{11}EO_{42}$ (M_w = 2110 g/mol), with a reactive methacrylate (MA) group at the end of the molecule, was synthesized according to a procedure described elsewhere.[27] The reactive group was utilized in the grafting reaction with VCL. The grafted copolymer PVCL-*g*-$C_{11}EO_{42}$ was prepared by the following procedure. The components VCL (18 g, 0.13 mol) and $MAC_{11}EO_{42}$ (3.6 g, 1.7 mmol) were dissolved in benzene (110 mL). The solution was degassed with nitrogen for 30 min at room temperature, after which it was heated to 70 °C. As soon as the polymerization temperature was reached, a solution of AIBN (50.4 mg in 10 mL of benzene) was injected into the reaction mixture. After 20 h, the mixture was cooled to room temperature, and the polymer was isolated by precipitation in hexane. The polymer was purified further by two reprecipitations from THF into hexane. To remove low molecular weight impurities, the polymer was thoroughly dialyzed against water (5 days) and isolated by freeze-drying. The structure and purity of the copolymer were ascertained by ^{1}H NMR with a 200 MHz Varian Gemini 2000 spectrometer (Palo Alto, CA): δ, (ppm, $CDCl_3$): 4.4 (1H), 3.7 (172 H), 3.4 (3H), 3.2 (2H), 2.4 (2 H), 1.2−2.0 (31H). The spectrum of PVCL-*g*-$C_{11}EO_{42}$ shows a well-separated peak at 3.7 ppm, corresponding to ethylene oxide of the macromonomer. The macromonomer content of the copolymer was determined to be 15 wt %, i.e., 1.2 mol % based on the relative peak areas at 3.7 and 4.4 ppm.

The reactivity of VCL is known to be quite low compared to other monomers, such as methacrylates,[37] and this may affect the randomness of the distribution of the grafted alkyl-poly(ethylene oxide) moieties along the chain. It may be expected, however, that the distribution of the grafts along the polymer backbone will be random, rather than "blocky", given the larger size of the macromonomer compared to VCL. Steric effects may offset the difference in the reactivity between the macromonomer methacrylate group and VCL.[38]

The molecular weight (M_w = 200 000) and second virial coefficient ($A_2 = 1.5 \times 10^{-4}$ mol mL g^{-2}) of PVCL-*g*-$C_{11}EO_{42}$ in aqueous solution were determined by intensity light scattering at 20 °C, and the data were analyzed by using the Zimm plot. The refractive index increment was 0.206 mL/g. The samples employed in the measurements were prepared by first weighing in the components and then stirring the solutions for 1 day at ambient temperature to ensure that the samples were homogeneous. In all experiments, the samples were allowed to equilibrate for at least 1 h at each measurement temperature before experiments were commenced. In all measurements, swelling and deswelling of the molecules or particles with temperature was fast and fully reversible, so that experimental problems, such as for example time-dependent effects, have not been observed. This simple behavior is similar to that reported[13] for aqueous solutions of poly(*N*-isopropylacrylamide) chains grafted with poly(ethylene oxide).

Turbidimetry. The turbidities and cloud points of the solutions were determined with the aid of an NK60-CPA cloud point analyzer from Phase Technology, Richmond, B.C., Canada. This instrument utilizes a scanning diffusive light scattering technique to characterize phase changes of the sample with high sensitivity and accuracy. A light beam (the peak wavelength of the utilized AlGaAs light source is at 654 nm, with a typical spectral half-width of 18 nm) is focused on the measuring sample. While directly above the sample, an optical system with a matrix of light-scattering detectors continuously monitors the scattered intensity signal of the sample as it is subjected to prescribed temperature alterations. The matrix is designed to cover the entire sample area. The test solution (0.15 mL) is applied by means of a micropipet onto a special designed glass plate that is coated with a thin metallic layer of very high reflectivity (mirror). To avoid evaporation of solvent at elevated temperatures, the sample surface is covered with 0.15 mL of highly transparent silicon oil (the density of the oil is lower than that of the sample). A platinum resistance thermometer probes the temperature of the sample, and very close to the test solution, a compact thermoelectric device (array of Peltier elements) is employed to cool and warm the sample over a wide temperature range of −60 to +60 °C. With this arrangement, the temperature can be changed very fast (up to 30 °C/min) and the cooling or heating rate can also be set to very low values. The instrument is interfaced to a PC, and the supplied software controls the operation of the turbidimeter and continuously collects data. In this work, the heating rate was set to 0.2 °C/min, and no effect of the heating rate on the signal was observed at low heating rates. The cooling (0.2 °C/min) of the samples was also checked to reveal possible hysteresis effects, but the corresponding cooling and heating curves always collapsed onto each other. In view of this, only heating curves are reported in this study.

The basic operation of the apparatus is illustrated in Figure 2. In Figure 2a, the measured signal of the scattered intensity from a dilute solution (0.02 wt %) of PVCL-*g*-$C_{11}EO_{42}$ is shown as a function of temperature. At approximately 33 °C, a steep rise of the signal occurs; i.e., the turbidity of the sample increases. The temperature at which the first deviation of the scattered light intensity from the baseline occurred was taken as the cloud point of the corresponding solution. To transform the signal into turbidity, we have measured the transmittance of the same solutions in a 1 cm cuvette with the aid of a spectrophotometer. The turbidity τ has been determined by using the expression $\tau = (-1/L)\ln(I_t/I_0)$, where L is the light path length of the cuvette, I_t is the transmitted light intensity, and I_0 is the incident light intensity. The relation between the calculated turbidity from the spectrophotometer experiments and the signal (S) from the cloud point analyzer is found to be given by the relationship τ (cm^{-1}) = $9.0 \times 10^{-9} S^{3.751}$ (see Figure 2b). An analogous turbidity plot to the signal plot (Figure 2a) is displayed in Figure 3c. Henceforth, all data from the cloud

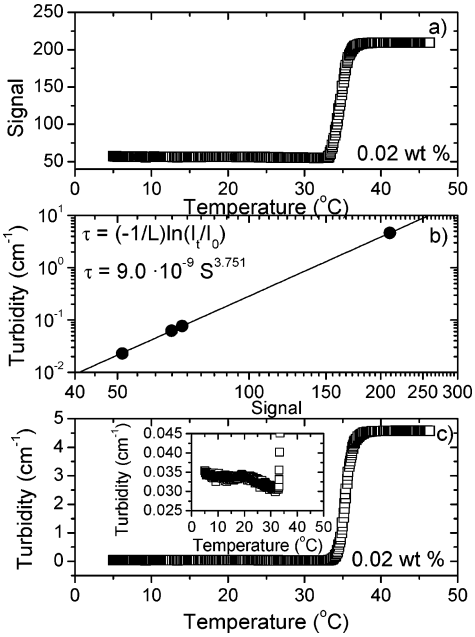

Figure 2. (a) Illustration of the temperature effect on the signal (scattered intensity) from the turbidity instrument for a dilute solution (0.02 wt %) of PVCL-*g*-$C_{11}EO_{42}$. (b) Relation between the turbidity measured from a spectrophotometer and the signal recorded from the cloud point analyzer (see text for details). (c) Calculated turbidity as a function of temperature for the 0.02 wt % solution. The inset is a magnification of the initial part of the turbidity curve (the details are discussed in the text).

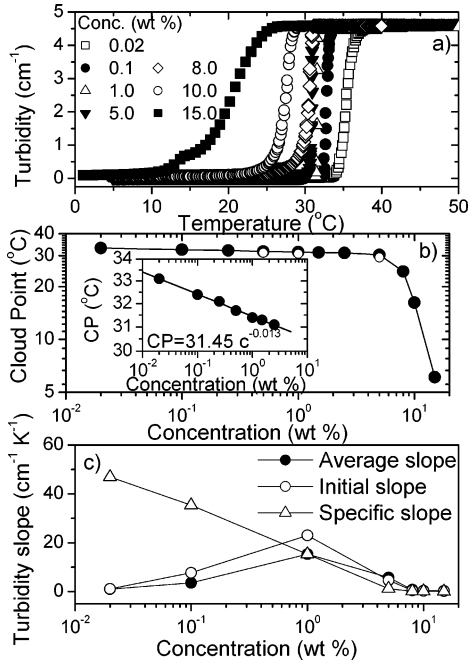

Figure 3. (a) Influence of polymer concentration on the turbidity behavior of aqueous solutions of PVCL-*g*-$C_{11}EO_{42}$. The cloud point is determined from the onset of the increase of the turbidity. (b) Effect of polymer concentration on the cloud point, and the open symbols show the cloud points with D_2O as solvent. The inset shows that in the dilute regime the concentration dependence of the cloud point can be described by a power law. (c) Slope of the turbidity change plotted vs concentration. The curve labeled "specific" is the average slope normalized to the concentration of each sample. The abscissa has been put on a logarithmic scale to better show the change at low concentrations.

point analyzer will be presented in terms of turbidity. This setup is powerful, giving an unusually high accuracy in the determination of the cloud point. For the present systems the values of CP are determined with an estimated accuracy of ±0.1 °C in the concentration range up to 5 wt %. The error in CP increases for the concentrations above this value (e.g., approximately ±0.5 °C at 8 wt %) due to the less abrupt turbidity change in the initial phase. It is interesting to note that a magnification of the initial part of the turbidity curve (see the inset plot of Figure 2c) for the 0.02 wt % solution discloses a small but clearly detectable decrease of the turbidity with increasing temperature. This is attributed to contraction (cf. the discussion below) of the polymer coils (reduced scattered intensity) before the enhanced stickiness of the entities at elevated temperature leads to intensive aggregation of the molecules and increased turbidity.

With the current setup it is also possible to identify the small change in cloud point that occurs when light water (H_2O) is substituted by heavy water (D_2O) as solvent. The cloud point is found to be slightly lower with D_2O; the difference is 1.0 °C at 1 wt % and 1.1 °C at 5 wt % concentration of the polymer.

Small-Angle Neutron Scattering (SANS). The SANS measurements were conducted at the IFE reactor in Norway. A liquid nitrogen cooled 15 cm long Be filter is installed in the beam path to remove fast neutrons (cutoff at a wavelength of $\lambda = 4$ Å), and additional 15 cm Bi filter removes the γ radiation. The wavelength was set by the aid of a selector (Dornier), using a high fwhm for the transmitted beam ($\Delta\lambda/\lambda = 20\%$) and maximized flux on the sample. The beam divergence was set by an input collimator (18.4 or 12.2 mm diameter) located 2.2 m from the sample, together with a collimator that was fixed to 4.9 mm. The neutron detector was a 128 × 128 pixel, 59 cm active diameter, ^{3}He-filled RISØ-type detector, which is mounted on rails inside an evacuated detector chamber. The distance was varied from 1.0 to 3.4 m and the wavelength between 5.1 and 10.2 Å, giving a wavevector range from 0.008 to 0.3 Å^{-1}. The wavevector q is given by $q = (4\pi/\lambda) \sin\theta$, where θ is the half of the scattering angle.

The polymer solutions were held in 2 mm quartz cuvettes, which were equipped with stoppers. The measuring cells were placed onto a cooper base for good thermal contact and mounted in the sample chamber. The experiments were carried out at different temperatures in the range 25−40 °C (temperature controlled to within ±0.1 °C). In all the SANS measurements, deuterium oxide was used as a solvent instead of light water to obtain good contrast and low background for the neutron-scattering experiments.

Standard reductions of the scattering data, including transmission corrections, were conducted by incorporating data collected from empty cuvette, beam without cuvette, and blocked-beam background. When relevant, the data were transformed to an absolute scale (coherent differential cross section ($d\Sigma/d\Omega$)) by calculating the normalized scattered intensity from direct beam measurements.[39]

Rheology. Oscillatory shear and viscosity measurements were performed in a Paar-Physica MCR 300 rheometer using a cone-and-plate geometry, with a cone angle of 1° and a diameter of 75 mm. This rheometer operates effectively with this geometry even on dilute polymer solutions, and the viscosity of water can easily be measured over an extended shear rate domain. The samples were introduced onto the plate, and to prevent evaporation of the solvent, the free surface of the sample was always covered with a thin layer of low-viscosity silicone oil. (The viscoelastic response of the samples is not observed to be affected by this layer.) The measuring unit is equipped with a temperature unit (Peltier plate) that provides a rapid change of the temperature and gives an accurate temperature control over an extended time for all the temperatures considered in this work. The values of the strain amplitude were checked to ensure that all oscillatory shear measurements were performed within the linear viscoelastic regime, where the dynamic storage modulus (G') and loss modulus (G'') are independent of the strain amplitude. The oscillating sweep measurements were carried out in the approximate angular frequency (ω) domain 0.1−100 rad/s.

The shear viscosity experiments were conducted over an extended shear rate range, and near Newtonian behavior was detected at all polymer concentrations and temperatures. The great accuracy of this powerful rheometer makes it appropriate for measurements on dilute solutions and the determination of the intrinsic viscosity [η]. The intrinsic viscosity is frequently determined with the aid of a capillary viscometer, but in that type of viscometer, the solutions are usually exposed to high shear rates (100−200 s^{-1}) that may induce shear thinning of the samples. Therefore, the viscosity measurements in the present work have been carried out on the rheometer at low shear rates.

Dynamic Light Scattering. Dynamic light scattering experiments were conducted with the aid of a standard laboratory built light scattering spectrometer with vertically polarized incident light of wavelength $\lambda = 514.5$ nm supplied by an argon ion laser (Lexel laser, model 95). The beam was focused onto the sample cell through a temperature-controlled chamber (temperature controlled to within ±0.05 °C) filled with refractive index matching silicone oil. The sample solutions were filtered at room temperature through 0.8 μm filters directly into precleaned 10 mm NMR tubes (Wilmad Glass Co.) of highest quality. By measuring the densities (by an Anton Paar DMA 5000 density meter, ±0.000 01 g/mL) of the solutions before and after filtration, it was checked that no polymer was adsorbed onto the filter.

In the present investigation the full homodyne intensity autocorrelation function $g^2(q,t)$ was recorded at different scattering angles and temperatures with an ALV-5000 multiple tau digital correlator. If the scattered field obeys Gaussian statistics, the measured correlation function $g^2(q,t)$ can be related to the theoretically amenable first-order electric field correlation function $g^1(q,t)$ by the Siegert relationship[40] $g^2(q,t) = 1 + B|g^1(q,t)|^2$, where B is usually treated as an empirical factor.

Both at low and higher polymer concentrations considered in this work, the decays of the correlation functions were always found to be bimodal at temperatures up to the CP, with initially a single exponential, followed at longer times by a stretched exponential

$$g^1(t) = A_f \exp(-t/\tau_f) + A_s \exp[-(t/\tau_{se})^{\beta}] \qquad (1)$$

with $A_f + A_s = 1$. The parameters A_f and A_s are the amplitudes for the fast and the slow relaxation mode, respectively. The same type of behavior was recently reported[13] in a DLS study of thermally responsive chain association in aqueous solutions of poly(*N*-isopropylacrylamide)-*g*-poly(ethylene oxide). The fast relaxation mode was ascribed to the diffusion of individual polymer coils, or small clusters of molecules, and the other mode was attributed to interchain aggregation. Above the CP, the correlation function is found to be unimodal, and the decay is described by a stretched exponential with a narrow distribution of relaxation times.

Analyses of the time correlation functions of the concentration fluctuations in the domain $qL < 1$, where L is a characteristic length (the hydrodynamic radius R_h in the dilute regime or the dynamic screening length ξ_h in the semidilute regime), have shown that the first term (short-time behavior) on the right-hand side of eq 1 is associated with the mutual diffusion coefficient D_m ($\tau_f^{-1} = D_m q^2$). The second term (long-time behavior) is expected to be related to disengagement relaxation of individual chains[41,42] or cluster relaxation.[43] In this study, the fast mode (the inverse fast relaxation time τ_f) is always diffusive (q^2), while the slow mode usually exhibits a stronger q dependence ($q^{2.5-3}$). The latter behavior indicates that large aggregates are formed, and the stronger q dependence is due to the contribution from internal modes. The variable τ_{se} in eq 1 is some effective relaxation time, and β ($0 < \beta \leq 1$) is a measure of the width of the distribution of relaxation times. The mean relaxation time for the slow mode is given by

$$\tau_s = \frac{\tau_{se}}{\beta}\Gamma\left(\frac{1}{\beta}\right) \qquad (2)$$

where $\Gamma(\beta^{-1})$ is the gamma function of β^{-1}.

In the analysis of the correlation function data, a nonlinear fitting algorithm (a modified Levenberg−Marquardt) was employed to obtain best-fit values of the parameters A_f, τ_f, τ_{se}, and β appearing on the right-hand side of eq 1. In addition, some of the results have been checked by utilizing the constrained regularized CONTIN method[44] in the analysis of the correlation functions (see below).

Results and Discussion

Turbidimetry and Cloud Points. Figure 3a presents typical turbidity curves for aqueous solutions of PVCL-*g*-$C_{11}EO_{42}$ of different polymer concentrations.

The characteristic feature of all the curves is the abrupt increase in turbidity at higher temperatures. It is evident that this transition is shifted toward lower temperatures as the concentration increases. Figure 3b shows a log−log representation of the effect of concentration on CP. In the dilute concentration regime (up to 2.5 wt %), the moderate decrease of CP with increasing polymer concentration (c) can be described by a power law relation CP (°C) = $31.45c^{-0.013}$ (see the inset plot), whereas in the semidilute regime CP falls off strongly as the concentration increases. As the temperature rises, the polymer molecules become more "sticky" (the hydrophobicity increases), and when they collide aggregates are formed, giving rise to enhanced turbidity. The depression of CP with increasing polymer concentration may be rationalized in terms of the Flory−Huggins interaction parameter on the form[45−47] χ_{eff}, where χ_{eff} is a function of both temperature (T) and concentration (c), i.e., $\chi_{eff} = \chi_{eff}(T,c)$. At a given temperature, the effective interaction parameter usually rises with increasing polymer concentration, and this trend is related to poorer solvent conditions or in the case of associating polymer solutions to stronger association. This issue has been addressed in several theoretical advances.[48−54] In the model by de Gennes,[50] the concentration dependence of χ_{eff} is ascribed to attractive interactions, giving rise to stable clusters of $n > 2$ monomers (e.g., micelles), while binary monomer−monomer interactions remain repulsive. This model predicts a situation at very poor thermodynamic conditions, where a dilute solution of individual coils coexists with a dense polymer phase (i.e., aggregates). A scenario emerges where increasing the polymer concentration reduces solvent quality; e.g., a solution of a polymer in water at room temperature exhibits good solvent features at low polymer concentration and poor solvent properties at high concentration. A modified version of the model proposed by de Gennes for PEO has recently been applied[54] to polysoaps and hydrophobically modified water-soluble polymers. An approach applicable to all polymer solutions was elaborated by Painter et al.[52] In this model, the concentration dependence of χ_{eff} is attributed to the interplay between intrachain and interchain contacts. In light of this discussion, the observed decrease of CP with rising polymer concentration can be ascribed to a more intense intermolecular association at higher concentration, leading to a reduction of the cloud point. The strong depression of CP detected in the semidilute regime can probably be traced

to the close contact between the molecules, and at this stage, a moderate temperature increase will trigger a rapid growth of aggregates.

It is evident from the plots in Figure 3a that the shape of the turbidity curve is different for the different concentrations. There seems to be a significantly lower slope at the onset of turbidity for the higher concentrations. We have therefore calculated the initial slope, here defined as the turbidity value at half-maximum divided by the temperature difference between this point and the onset of turbidity, and also the average rate, defined as the total turbidity change divided by the temperature difference between the maximum value and the onset. These data are plotted in Figure 3c. There is a marked change of the slope as the concentration is increased from 0.02 wt % and upward. However, at 1 wt % there is a distinct maximum showing the very abrupt change seen for this concentration (Figure 3a). The turbidity changes initially more than 15 cm^{-1} K^{-1} at this concentration, and the solution changes from transparent to turbid over a range of only 0.4 °C. At higher concentrations the slope is again reduced. However, if these data are normalized with respect to the polymer concentration, a different picture emerges (curve labeled specific in Figure 3c). Now there is a continuous slope change from about 47 cm^{-1} K^{-1} wt $\%^{-1}$ at 0.02 wt % to 0.01 cm^{-1} K^{-1} wt $\%^{-1}$ at 15 wt %, showing that the peak at 1 wt % is principally a concentration effect. The reason is that the reduction in the amount of reflected light (i.e., turbidity) in the experimental setup will at any temperature be directly related to the concentration of polymer in the sample volume.

We explain the slope change from low to high concentrations in the following way. At high concentrations, the chains are close to each other, and there may even be some smaller aggregates present at low temperatures. Only a little change in hydrophobicity, taking place already at moderate temperatures, is necessary to increase the probability of a chain adhering to a nearby chain or connecting to an already existing aggregate. At low concentration, this is much less probable, and large aggregates are not formed until the sticking probabilities of the chains are at their maximum, i.e., very close to the cloud point, thus creating a sharp transition.

SANS Results. In SANS experiments, probing a wide q domain provides a wealth of information on the structure of the solution over a range of length scales. This is especially true in the case of associating polymer systems in which both single-chain and multichain characteristics are involved. The q dependences of the scattered intensity for a dilute (1.0 wt %) and semidilute solution (5.0 wt %) of PVCL-g-$C_{11}EO_{42}$ at various temperatures are depicted in Figure 4. The results reveal an upturn of the scattered intensity at low q values that is strengthened with increasing temperature. As expected, a significantly higher intensity is obtained for the higher polymer concentration. At low temperatures, the scattering curves show tendencies of a plateau at low q, whereas at higher temperature a progressively stronger upturn of the scattering curves at low q appears. This behavior can be explained by the formation of large association structures.

The q dependence of the scattering at high q is related to the degree of compactness of the polymer structures. The SANS data for the current system show significant

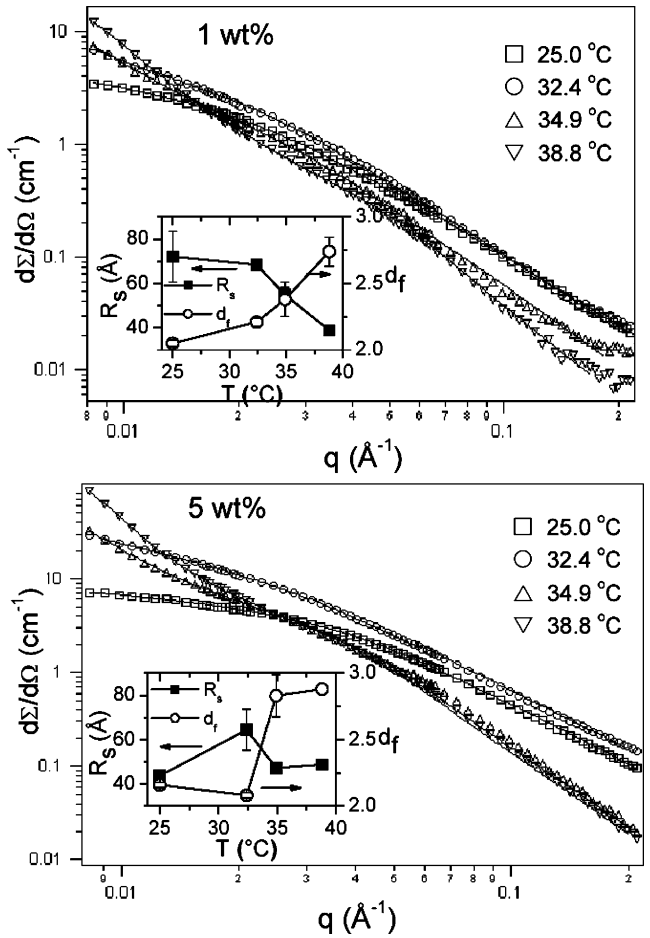

Figure 4. SANS intensity plotted vs the scattering vector q at two polymer concentrations and at different temperatures for the PVCL-g-$C_{11}EO_{42}$/D_2O system. The incoherent background has been subtracted from the data. The data have been fitted (continuous line) to the extended Beaucage model[55,56] for each temperature (see eq 4). The insets show the mass fractal dimension and the size of the corresponding substructure as extracted via the Beaucage model.

variation in the high-q behavior, and standard models (sphere, core−shell) did not provide good fit to the data. This is probably because the PVCL-g-$C_{11}EO_{42}$ chains do not assemble into well-defined, compact particles, but rather into structures that have a more irregular surface (with high content of the hydrophilic side chains) and a varying packing density as one moves from the outside toward the core of the particles.

Recently, Beaucage[55,56] has proposed a model for scattering that involves a variable mass fractal, applicable also to polymeric systems:

$$I(q) = G \exp\left(-\frac{q^2 R_g^2}{3}\right) + B\left(\frac{1}{q^*}\right)^{d_f} \qquad (3)$$

where $q^* = q/[\mathrm{erf}(qkR_g/\sqrt{6})]^3$. Here, erf is the error function, and G and B are amplitudes, related to each other as $B = Gd_f/R_g^{d_f}\Gamma(d_f/2)$. The parameter d_f is the mass fractal dimension of the structural level described by eq 3 and of size R_g, Γ is the gamma function, and k is an empirical constant, equal to 1.06. There are thus three free parameters in this model: G, R_g, and d_f. In eq 3, the first term can be identified as that corresponding to a conventional Guinier approach, whereas the second term describes the scattering at higher q values, i.e., the contribution from the internal structure of the

scattering particles, taking into account that these structures may have varying degree of compactness. The model described by eq 3 will produce a scattering profile that reaches a plateau in the low-q region (when $qR_g < 1$). However, very often an additional increase in the scattering is seen at low q, indicating the presence of also larger structures in the solution. One may then make use of the fact that the Beaucage model can be extended to include scattering from different structural levels. In a situation where there are two different length scales/structural levels present, the model will take the form[56,57]

$$I(q) = G\exp(-q^2R_g^2/3) + B\exp(-q^2R_s^2/3)(1/q^*)^{D_f} + G_s\exp(-q^2R_s^2/3) + B_s(1/q_s^*)^{d_f} \quad (4)$$

where $q_s^* = q/[\mathrm{erf}(qkR_s/\sqrt{6})]^3$. The first term in eq 4 is again the Guinier part of large scale structures of size R_g supposed to be composed of smaller building blocks of size R_s, expressed in the third term. The second term describes the mass fractal behavior of the largest structures (fractal dimension D_f), with the lower/higher scale limits R_s and R_g, controlled by the error function and the exponential prefactor, respectively. The final term, effective only at high q, describes the internal fractal behavior of the smallest scale structures (exponent d_f). The function of eq 4 thus contains a total of six free parameters. The SANS data obtained on our polymer solutions were fitted to the Beaucage model of eq 4, and the corresponding fits are shown with continuous lines in Figure 4. The fractal dimensions for the substructures as well as their size are shown in the insets of Figure 4. One has to be cautious when introducing many parameters for making fits to experimental data, since one can easily achieve a good fit using a wrong model, but with a sufficient number of parameters. On the other hand, the extended Beaucage model (eq 4) is introduced here only to improve the description in the low-q region. It has very little influence in the intermediate and high-q region where one can extract the mass fractal dimension of the substructures.

The value of d_f for both polymer concentrations is found to increase as the solutions are heated through the cloud point. The change is from approximately 2.0 to 2.7 for the 1 wt % and from 2.1 to 2.9 for the 5 wt % system as the temperature is changed from 25 to 39 °C. The fractal dimension of the polymer chains is related to the Flory excluded-volume exponent ν ($R_g \sim M^\nu$), defined as $\nu = 1/d_f$. The theoretical predictions[58] for the self-avoiding linear chain and the Gaussian chain are $d_f = 1.7$ ($\nu = 0.59$) and $d_f = 2$ ($\nu = 0.50$), respectively. For more condensed structures that can be formed as the critical solution temperature is reached ($\nu = 0.33$) d_f can attain values up to 3 (globule). The observed trend of d_f suggests that the clusters are swollen at low temperatures, but as the temperature increases, structures that are more compact are formed. This is a result of deteriorated thermodynamic conditions with rising temperature—from good to poor solvent conditions.

The size of the substructures (R_s) found when employing the Beaucage model (eq 4) is seen to decrease considerably for the 1 wt % system, from about 70 Å to 40 Å, when the temperature rises. This effect is reasonable if one considers each substructure as a unit consisting of a given number of polymer chains. These structures are expected to contract with increasing temperature. For the high concentration (5 wt %) the trend is not clear. It should be mentioned that the Beaucage equation is essentially a form factor, thus well correlated with the scattered intensity only if the structure factor of the system is close to 1. This may not be totally true when entering the semidilute regime (5 wt %). The largest scale structures, the presence of which are indicated by the significant increase in low-q scattering at higher temperatures, are not expected to be well described, since there is little sign of a low-q plateau, apart from maybe at the lowest temperature. We obtain values for R_g of 190 Å (1 wt %) and 150 Å (5 wt %) at 25 °C. A clear increase, by a factor of about 2 but with large uncertainty, is seen as the cloud point is passed. The smaller value of R_g for the higher concentration at 25 °C is probably an indication of the thermodynamic conditions becoming poorer at higher polymer concentration, as this leads to a reduction in the overall size of the molecules. At higher temperatures, this tendency is concealed by interchain association. This effect is probably responsible for the fact that the average cluster size increases as the CP is passed.

The extrapolated intensity value for zero angle scattering ($q = 0$) can in principle be used to calculate an apparent molecular weight since the cross section (cm^{-1}) can be written as $d\Sigma(q=0)/d\Omega = [c(\Delta r_{SLD})^2/(\rho^2 N_A)]M_W$. Here c is the polymer concentration, Δr_{SLD} is the difference in scattering length density between the polymer particle and the solvent, and ρ is the mass density of the polymer. Using such an analysis on the SANS pattern that shows indications of a plateau in the low-q range, i.e., 1 wt % at 25 °C sample, gives an apparent M_W of approximately 40 000—considerably lower than what was obtained from light scattering. Although both Δr_{SLD} and ρ are difficult to estimate accurately (both depend on the actual conformation of the polymer in solution), this difference is another indication that we do not probe fully the scattering behavior at the smallest angles and that the scattered intensity continues to increase below the q limit accessible in the current setup.

The fact that the samples, by visual inspection, are seen to change from transparent to grayish as the CP is passed is also a clear demonstration of the formation of large structures, even beyond the 1000 Å range.

Rheological Properties. In Figure 5a,b, the frequency dependencies of the storage (G') and the loss (G'') modulus for three polymer concentrations at two different temperatures are illustrated. It is shown that $G'' > G'$ at all conditions over the considered angular frequency domain, reflecting the liquidlike response of these solutions. We note that the values of G' rise with increasing polymer concentration.

A procedure to analyze dynamic moduli data has recently been proposed.[59,60] In this approach, it was noted that if the loss modulus is plotted as a function of the storage modulus, a linear relation in a log−log plot is obtained. The value of the power law exponent e ($G'' \sim (G')^e$) is equal to 0.5 if the viscoelastic response of the system can be described by a single Maxwell element. This type of plot can be utilized to characterize deviations from the Maxwell model. Details of this procedure have been discussed elsewhere.[60] Plots of this type are displayed in Figure 5c,d, and at all conditions the data can be represented by straight lines over the considered angular frequency domain. The values of e are close to 1, suggesting that these systems deviate from the simple Maxwellian response. This shows that

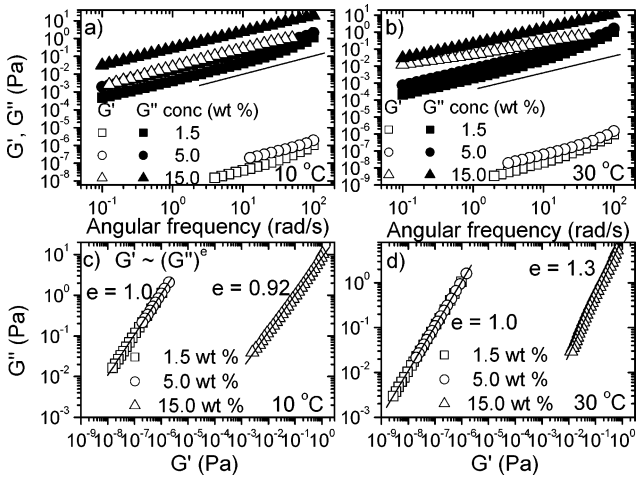

Figure 5. (a, b) Frequency dependencies of the dynamic moduli for the PVCL-*g*-$C_{11}EO_{42}$/H_2O system at the temperatures and polymer concentrations indicated. The continuous line below the data points are that of a Maxwellian model for G'' with a single relaxation constant in the low-frequency regime. (c, d) log−log plots of G'' vs G' for solutions of PVCL-*g*-$C_{11}EO_{42}$/H_2O of different polymer concentrations and temperatures (see text for details).

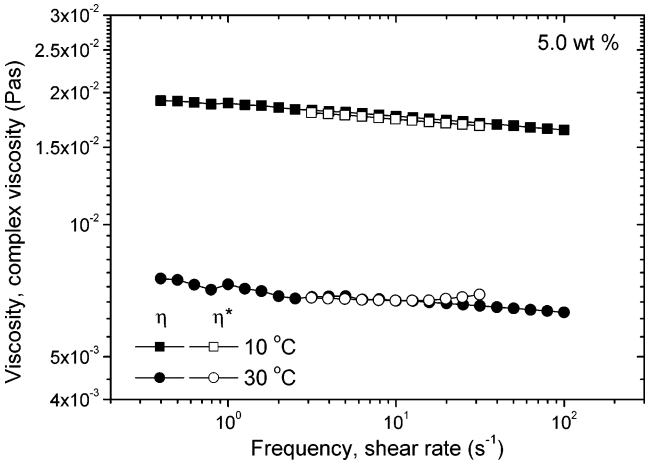

Figure 6. Shear viscosity compared to the magnitude of the complex viscosity for aqueous solutions of PVCL-*g*-$C_{11}EO_{42}$ plotted in the same graph for two different temperatures.

the relaxation process of the polymer systems is not controlled by a single mode, but a broad distribution of relaxation modes.

In Figure 6, both the complex viscosity η^* and the shear viscosity η have been plotted for two different temperatures, far from the cloud point (10 °C) and close to the cloud point (30 °C). The two measurement methods give similar results in the frequency domain studied; thus, the Cox−Merz rule seems to be fulfilled for the present system.

A typical feature of many associated and/or entangled polymer solutions is a strong shear dependence of the viscosity. The effect of shear rate on the measured viscosity for solutions of PVCL-*g*-$C_{11}EO_{42}$ of different polymer concentrations and at various temperatures is displayed in Figure 7. A Newtonian behavior of the viscosity appears over the studied shear rate range at all conditions, except for the higher two concentrations (10 and 15 wt %) where a weak shear thinning effect is visible. This finding and the relatively low viscosities of these solutions indicate that no interconnected network structures are formed even at high polymer

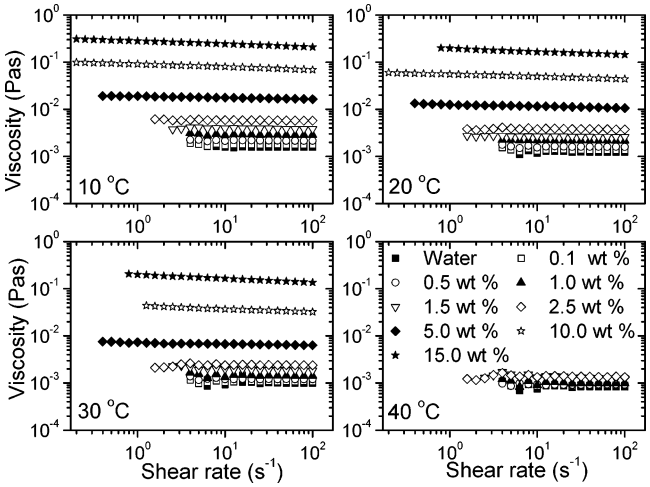

Figure 7. Effects of polymer concentration and temperature on the shear rate dependence of the viscosity for aqueous solutions of PVCL-*g*-$C_{11}EO_{42}$.

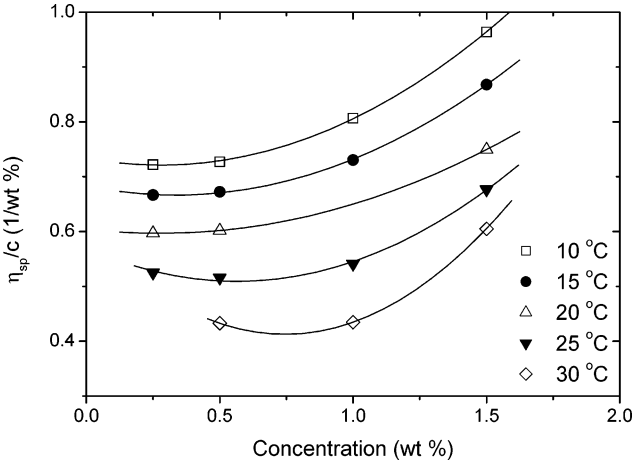

Figure 8. Reduced viscosity as a function of polymer concentration for aqueous solutions of PVCL-*g*-$C_{11}EO_{42}$ at the temperatures indicated. The data points have been fitted to a second-order polynomial.

concentration, but there may still be present interaction between particles. The small shear thinning effect at high concentrations suggest that the interchain structures are quite stable against shear. Such a weak shear dependence of the viscosity does not seem to be a common feature for this kind of system because strong shear thinning has been reported[61] for colloidal dispersions of core−shell particles. Furthermore, in solutions of associating polymers forming networks, strong shear thinning effects are often observed.[62−65] At high temperatures (40 °C; well above CP), the low-viscosity data for the solutions in the dilute concentration regime (cf. Figure 7) suggest contraction of the clusters and molecules, whereas at higher polymer concentrations the polymer precipitates and hence the results are not displayed.

The concentration dependences of the reduced viscosity $\eta_{red} \equiv \eta_{sp}/c$ (η_{sp} is the specific viscosity and c the polymer concentration (weight fraction)) at different temperatures for dilute solutions of PVCL-*g*-$C_{11}EO_{42}$ are illustrated in Figure 8. This system shows a clear deviation from the linear behavior suggested by the Huggins' equation ($\eta_{red} = [\eta] + k_H[\eta]^2c$) for a nonionic polymer. There is a stronger dependence on c, indicating a stronger interchain interaction than in the Huggins

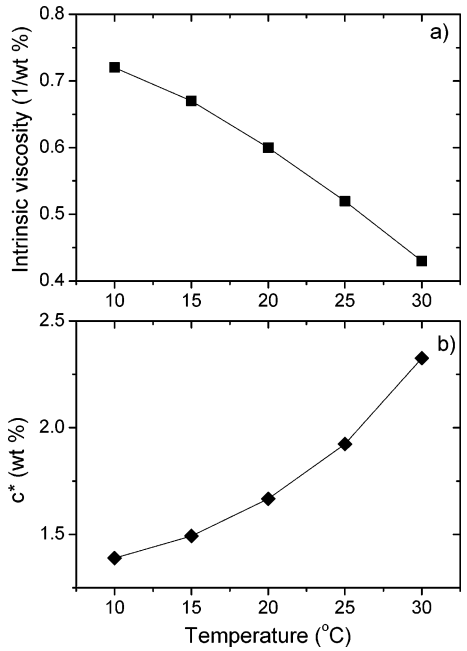

Figure 9. Temperature dependencies of the intrinsic viscosity and the overlap concentration c^*, defined by $c^* = 1/[\eta]$ for solutions of PVCL-*g*-$C_{11}EO_{42}$.

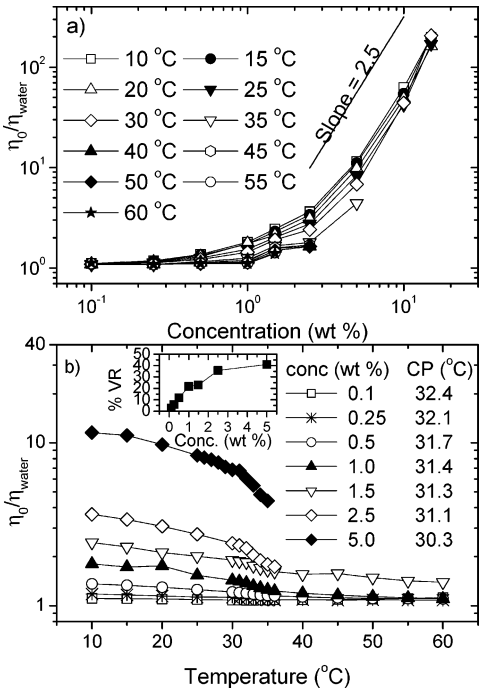

Figure 10. Concentration and temperature dependencies of the relative viscosity for solutions of PVCL-*g*-$C_{11}EO_{42}$. CP for each concentration is indicated. The inset in (b) shows the percentage decrease of the relative viscosity (% VR) up to CP as a function of polymer concentration.

model. This effect is strongest close to the cloud point (30 °C). This behavior supports the evolution of enhanced intermolecular association. Figure 9a shows that $[\eta]$ decreases monotonically with increasing temperature in the interval 10−30 °C. This is a clear evidence of that the molecules in dilute solution contract strongly upon heating. Because of this temperature-induced shrinkage of the moieties, the overlap concentration c^*, estimated from $c^* = 1/[\eta]$, rises with increasing temperature (see Figure 9b).

Figure 10a shows plots of the relative viscosity η_{rel} ($\eta_{rel} \equiv \eta_0/\eta_{water}$, with η_{water} the solvent viscosity) at different temperatures vs polymer concentration. Because of polymer precipitation, data for the highest concentrations have only been collected up to 30 °C. It is clear that the temperature has little influence at low polymer concentrations (up to 0.5 wt %). In the semidilute regime, a pronounced concentration dependence of η_{rel} is found, and this behavior can approximately be described by a power law $\eta_{rel} \sim c^x$ with $x \approx 2.5$. The theoretical prediction for the concentration dependence of η_{rel} for flexible nonassociating neutral polymers in unentangled semidilute polymer solutions is given by[66] $\eta_{rel} \propto c^{1/(3\nu-1)}$, yielding $\eta_{rel} \propto c^{1.3}$ in a good solvent ($\nu = 0.59$) and $\eta_{rel} \propto c^2$ in a θ solvent ($\nu = 0.50$). A stronger concentration dependence of η_{rel} is predicted for entangled polymer solutions, with $\eta_{rel} \propto c^{3/(3\nu-1)} \propto c^{3.9}$ at good solvent conditions[67] and $\eta_{rel} \propto c^{4.7}$ at θ conditions.[68] In semidilute solutions of associating amphiphilic polymers, most of the experimental studies[65,69−71] suggest strong concentration dependence of η_{rel} with values of x in the range from typically 3−7. In light of earlier experimental investigations and theoretical findings, the value of x for the present system suggests that despite high concentrations ($c[\eta] \approx 7$ for the highest concentration) the polymer chains in the solutions are unentangled. In this context it is interesting to note a recent rheological investigation[72] on soft colloidal particles, where a value of $x = 2.5$ was reported. This resemblance, together with the low absolute value and constancy of viscosity with shear rate (Figure 7), lends support to the conjecture that the solutions contain intrachain and interchain structures, but no interconnected network is formed. The dominance of one or the other of the structures in solution will depend on the polymer concentration and/or temperature.

The effect of temperature on η_{rel} for various polymer concentrations is illustrated in Figure 10b. The general trend is that the relative viscosity decreases with increasing temperature, and this effect becomes stronger at higher concentrations. The inset in Figure 10b shows the decrease of η_{rel} in percentages (% VR) in the temperature interval from 10 °C to CP for the considered polymer concentrations. The effect is seen to be more pronounced as the polymer concentration increases. A temperature and concentration increase evokes a situation with an intricate interplay between the phenomena of collapse and intermolecular aggregation. Poorer thermodynamic conditions lead to contraction of single chains and clusters, but on the other hand, the sticking probability increases because the particles become more hydrophobic and the frequency of "contact" due to Brownian fluctuations will be augmented as the polymer concentration increases and the formation of aggregates is promoted. The results shown in the inset plot seem to indicate that compression of the structural units play a dominant role during the temperature increase toward CP. At high polymer concentration, intermolecular association gives rise to the formation of aggregates, and the number density of PVCL chains in the interior of the structure is high, which strengthens the temperature-induced compression of the particles. This contraction can probably explain the pronounced drop of the relative viscosity at elevated temperatures for the higher concentrations.

Dynamic Light Scattering. Figure 11 shows normalized time correlation function data at a scattering angle of 90° for aqueous PVCL-*g*-$C_{11}EO_{42}$ solutions of

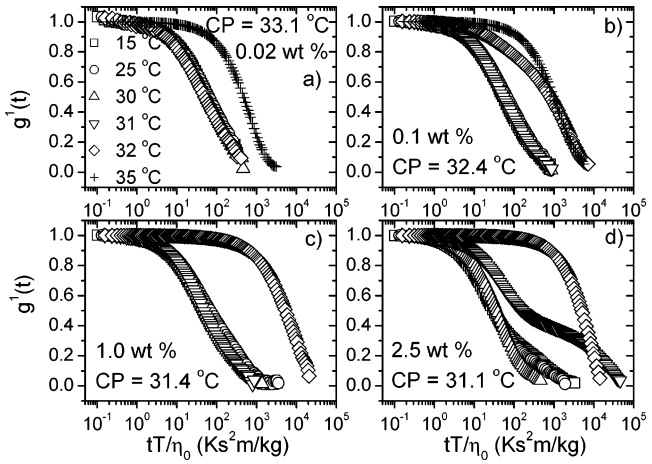

Figure 11. First-order field correlation function (at a scattering angle of 90°) vs the quantity tT/η_0 (trivial changes of the solvent viscosity with temperature are thereby accounted for) for solutions of PVCL-*g*-$C_{11}EO_{42}$ at the polymer concentrations and temperatures indicated.

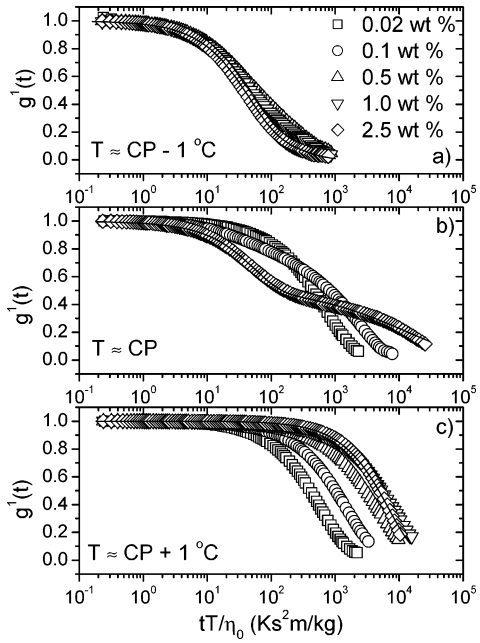

Figure 12. First-order field correlation function (at a scattering angle of 90°) vs the quantity tT/η_0 for solutions of PVCL-*g*-$C_{11}EO_{42}$ at the polymer concentrations and distances from the cloud point of each solution indicated. The lines show the fitted curves for the highest concentration, fitted with the aid of eq 1 before and at CP, and to a stretched exponential at CP + 1 °C.

various concentrations and different temperatures. By plotting the correlation function data against the quantity tT/η_0, trivial changes of the solvent viscosity with temperature have been taken into account. The general picture that emerges is that up to approximately the cloud point the effect of temperature on the relaxation at longer times is modest, whereas above CP the relaxation is slowed down and the profile of the correlation function is significantly altered.

The effect of polymer concentration on the decay of the correlation function at different distances from the CP is depicted in Figure 12. At CP and temperatures below, for each concentration the correlation functions can be well fitted with the aid of eq 1 (two relaxation modes) for all polymer concentrations, whereas at temperatures slightly above CP (CP + 1 °C) the decay

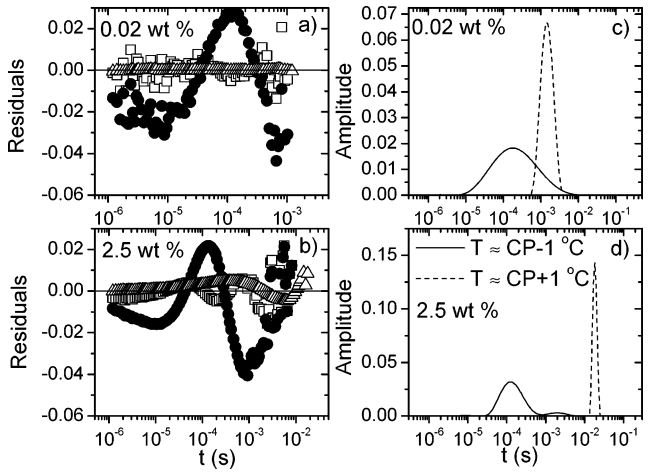

Figure 13. (a, b) Residuals obtained from fits of the correlation functions for the lowest (0.02 wt %) and highest (2.5 wt %) polymer concentration at temperatures close to CP (CP − 1 °C and CP + 1 °C). At CP − 1 °C, the small and random residuals (□) are obtained from fits with the aid of eq 1, whereas the large and systematic residuals (●) obtained from fitting the correlation function data by means of a single stretched exponential reveal that this functional form gives a poor description of the correlation functions at this condition. At CP + 1 °C, a narrow unimodal relaxation mode is found that is described by a single stretched exponential (△), which gives a good portrayal of the correlation functions. (c, d) CONTIN representations of the correlation functions at the same conditions. See text for more details.

can for all concentrations be well described by a single stretched exponential (one relaxation mode) with a high value (0.9−1) of β (narrow distribution of relaxation times). The contribution from the slow mode is stronger at CP (Figure 12b) than at lower temperatures, and its influence increases with increasing polymer concentration. At (CP + 1 °C), the decay time for the unimodal relaxation process is shifted toward higher values as the concentration rises (Figure 12c). This suggests that at this temperature condition the interchain association is promoted, and the clusters grow as the polymer concentration increases.

To scrutinize the goodness of the fitting procedures, and to endorse the functional forms of the fitting algorithms that we have used to portray the decays of the correlation functions at different conditions, residual plots and CONTIN[44] analyses for two polymer concentrations at different distances from CP are displayed in Figure 13. The random distribution and small values of the residuals obtained from the fitting, by means of eq 1, of the correlation function data for the two polymer concentrations below CP (CP − 1 °C) indicate a good agreement between the fitting expression and the experimental data. However, if an unimodal distribution of relaxation times is assumed and a single stretched exponential is fitted to the correlation function data up to CP, the large values and the systematic trends in the residuals disclose that this is a poor fit of the data (cf. Figure 13a,b). Thus, the decays of the correlation functions at conditions up to CP are best described by a bimodal relaxation process. The CONTIN representations at CP − 1 °C (see Figure 13c,d) reveal a single mode for the low polymer concentration and a bimodal distribution of relaxation times for the higher concentration, but the second mode is very weak. At the low concentration, the CONTIN regularization method comes up with a single broad peak because the relaxation modes are rather close to each other and the CONTIN

method is not capable of resolving the modes. Even at the high polymer concentration, the CONTIN method encounters problem in separating the two modes. This finding demonstrates that caution must be exercised when the CONTIN method is employed in the analysis of correlation function data.

Above the cloud point (CP + 1 °C), both the analysis of residuals and the CONTIN representation (a single narrow peak) are in favor of a unimodal relaxation mode with a narrow distribution of relaxation times for all polymer concentrations. Thus, for a given polymer concentration, the size distribution of the entities is rather narrow. At low concentration, collapsed molecules (globules) are formed, whereas at higher concentrations interchain association gives rise to the appearance of larger particles with the hydrophobic parts likely to be hidden within the core. At still higher temperatures, large aggregates are progressively formed, and through the macroscopic phase separation process the polymer eventually precipitates. We may note that, in a recent DLS study[30] on dilute solutions of thermoresponsive PVCL-*graft*-poly(ethylene oxide) copolymers above CP, a similar narrow unimodal relaxation mode was reported. The difference in the profiles of the correlation functions at temperatures up to CP, and slightly above this temperature, can be rationalized in the following scenario. Up to CP, one mode of the bimodal relaxation process is ascribed to the diffusion of individual polymer coils, or small clusters of molecules, and the other mode is attributed to interchain aggregation where aggregates may be formed with a hydrophobic interior (PVCL) and the surface covered by mainly PEO chains. Above CP, the enhanced stickiness of the individual polymer chains will promote multichain association and formation of clusters. As a result, the population of individual chain molecules will disappear, and the bimodal relaxation process is replaced by a unimodal relaxation.

Since the fast mode is diffusive, the apparent hydrodynamic radius R_h can be determined in the dilute concentration regime from the diffusion coefficient D via the Stokes−Einstein relationship

$$D = \frac{k_B T}{6\pi\eta R_h} \tag{5}$$

where k_B is the Boltzmann constant. In Figure 14a, the temperature dependence of R_h for different polymer concentrations is shown. This illustration unveils a number of noteworthy features. To obtain a clearer picture of the behavior before CP, a magnification of this area is displayed in the inset plot. It is here important to take into consideration the competition between intrachain and interchain associations. At a fixed low temperature (e.g., 15 °C), R_h is seen to decrease with increasing polymer concentration, and at this temperature stage the intermolecular aggregation is reduced and intrachain structures prevail. As discussed above, a concentration increase at a given temperature promotes poorer thermodynamic conditions of the system, and reduced excluded-volume effects generate contraction of the polymer molecules. A concentration-induced shrinkage of polymer molecules has also been observed[30] in aqueous solutions of thermoresponsive poly(*N*-isopropylacrylamide) chains grafted with poly(ethylene oxide) and for dilute solutions of PVCL.[26] On the other hand, we notice a growth of R_h with increasing concentration at an elevated temperature because the sticking probability rises, and the formation of interchain aggregates becomes an essential feature. For the lowest polymer concentration (0.02 wt %), a temperature-induced collapse of the molecules is registered below the CP, whereas at the highest concentration R_h rises steadily with increasing temperature. The former finding results from intrachain association and is supported by the constancy of the reduced intensity (Figure 14b) for this concentration at temperatures up to CP. The growth of R_h with increasing temperature at the highest concentration is ascribed to the enhanced interchain association, which is accompanied by a monotonic increase of the reduced intensity. At temperatures well above CP, both R_h and the reduced intensity display drastic temperature-induced upturns for all concentrations, suggesting formation of large aggregates.

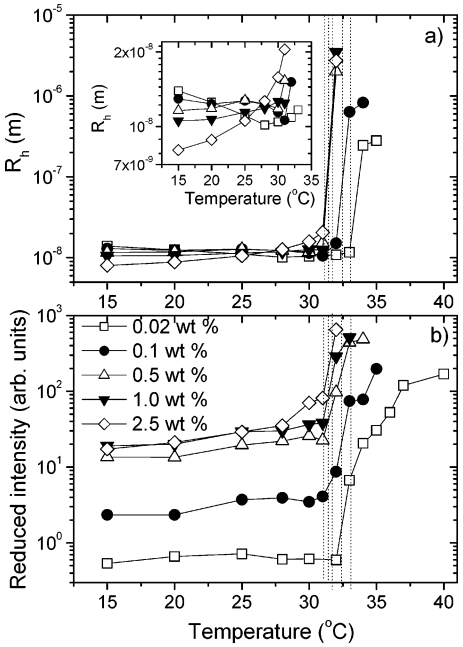

Figure 14. (a) Temperature dependencies of the apparent hydrodynamic radius, calculated from the fast relaxation mode, for solutions of PVCL-*g*-$C_{11}EO_{42}$ at the polymer concentrations indicated. The vertical lines indicate the cloud points for the different polymer concentrations, with the lowest CP for the highest concentration. The inset shows a magnification of the data up to CP. (b) Reduced scattered intensity as a function of temperature for solutions of PVCL-*g*-$C_{11}EO_{42}$ at the polymer concentrations indicated.

Figure 15a shows the combined effect of temperature and concentration on the hydrodynamic radius. Here one can see clearly a concentration-induced contraction of the coils at low temperatures and an enhanced interchain association and growth of aggregates at elevated temperatures. The effect of concentration on R_h at conditions close to the cloud point is depicted in Figure 15b. Just below CP and at CP, the value of R_h is practically independent of the concentration, whereas above CP large particles are formed, which continue to grow as the polymer concentration increases. These results for the fast mode demonstrate that the sizes of the molecules or clusters at CP − 1 °C and CP are almost the same, and the effect of polymer concentration at these conditions is negligible. The reason for this behavior is probably that just before and at the cloud point the thermodynamic conditions are already so poor that they will not be significantly deteriorated by increasing the polymer concentration, and therefore the

Table 1. A Concise Summary of the Main Observations with the Four Different Experimental Techniques Used[a]

turbidity	CP ↓ when c ↑	drastic change for c > 2.5 wt %	transition more abrupt when c ↓	
SANS	I(low q) ↑ when c, T ↑	R_g ↑ when T ↑; R_s ↓ when T ↑ (1 wt %)	R_g lower for 5 wt % than for 1 wt % at RT	d_f: 2.0→2.7 (1%); 2.1→2.9 (5%)
rheology	not single Maxwellian response	no shear thinning at any T (c < 10 wt %)	low viscosity values	[η] ↓ when T ↑
DLS	τ (long times) ↑ at CP	two τ's for $T \leq$ CP; one τ (stretched exp) for $T >$ CP	R_h (low T) ↓ when c ↑	R_h ↑ when T ↑, excl 0.02 wt %, where R_h ↓.

[a] The signs ↑ and ↓ mean "increasing" and "decreasing", respectively. The symbol I stands for intensity, and τ for the relaxation constant in DLS measurements. RT is room temperature.

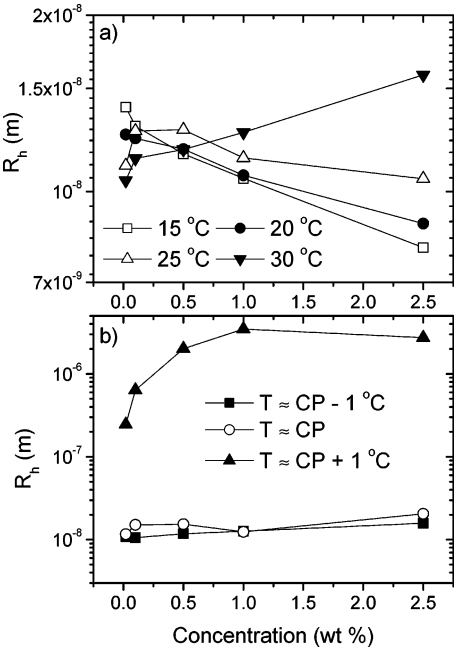

Figure 15. (a) Effects of concentration and temperature on the apparent hydrodynamic radius, calculated from the fast relaxation mode. (b) Concentration dependencies of R_h at different distances from the cloud point.

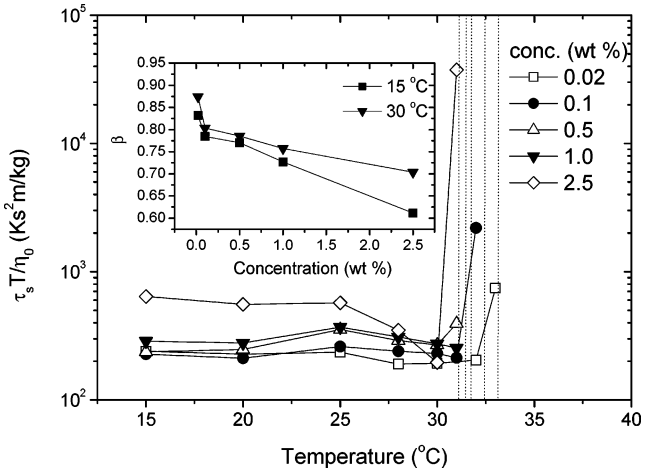

Figure 16. Effects of temperature and polymer concentration on the reduced slow relaxation time for solutions of PVCL-*g*-$C_{11}EO_{42}$ at the polymer concentrations indicated. The vertical lines indicate the cloud points for the different polymer concentrations, with the lowest CP for the highest concentration. The inset shows the effects of polymer concentration and temperature (temperatures below CP) on the stretched exponent β.

size of the molecules will not be significantly affected by concentration. At CP + 1 °C, strong interchain associations will lead to the formation of large particles whose growth is favored by increasing the polymer concentration. At this stage, the stickiness of the polymer segments is high, and a rather narrow distribution of interchain structures is formed.

Figure 16 shows the effects of temperature and polymer concentration on the reduced slow relaxation time for PVCL-*g*-$C_{11}EO_{42}$ solutions. Since this mode is not diffusive as the fast mode, but exhibits approximately a q^3 dependence, the results are not presented in terms of a hydrodynamic radius. This stronger q dependence is typical of the well-known scattering dependence found for very large molecular weight polymer coils[73,74] and for different types of loose polymer aggregates.[75,76] In this regime, the entities probed can no longer be considered as point scatters, and internal chain motions of length scale q^{-1} are monitored.[58] The large aggregate size of the particles giving rise to this relaxation mode ensures that $qR_{agg} > 1$. The salient features in Figure 16 are the rise of the reduced slow relaxation time with increasing polymer concentration and the strong upturn of the relaxation time as CP is approached. As expected, this effect is more marked as the concentration increases. The former feature announces the growth of multichain association complexes as the polymer concentration increases, and the latter behavior reflects the temperature-induced formation of large clusters. The inset plot shows the variation of the stretched exponent β with polymer concentration at two different temperatures. In both cases, the width of the distribution of relaxation times becomes broader as the concentration increases, but the effect is less pronounced at 30 °C for the higher concentrations. This may be because the higher concentrations at this temperature are closer to the situation where the two relaxation modes are replaced by a single narrow relaxation mode.

To help in the interpretation the data and to obtain a survey of the results from this work as a whole, a concise summary of the main observations is given in Table 1.

Conclusions

Interactions in aqueous solutions of the thermoresponsive PVCL-*g*-$C_{11}EO_{42}$ copolymer have been characterized by using different experimental techniques. The main results can be summarized in the following way. (i) The cloud point is shifted toward lower temperatures as the polymer concentration increases, and the depression is significantly stronger in the semidilute regime. (ii) The SANS results reveal that the upturn of the scattered intensity at low q is promoted by increased temperature and polymer concentration. This trend supports the surmise that high polymer concentration and elevated temperature favor the growth of interchain aggregates. The SANS data at higher q values suggest a gradual conformational transition from random coils to globule-like structures in the dilute concentration regime as the temperature rises. (iii) The dynamic moduli, recorded in the terminal zone of the mechanical spectrum, cannot be fitted to a single Maxwell element,

but the relaxation process is characterized by a broad distribution of relaxation times. The marked drop of the intrinsic viscosity with increasing temperature indicates a temperature-induced contraction of the molecules. The relative viscosity η_0/η_{water} falls off with increasing temperature, and this effect is more pronounced at higher concentrations. At high concentration, the number density of PVCL chains in the interior of the aggregate is high, and this promotes a strong contraction of the structures. The concentration dependence of the relative viscosity in the semidilute concentration regime can be described by the approximate power law $\eta_0/\eta_{water} \sim c^{2.5}$. This low value of the power law exponent, together with the low values of the viscosity and the modest shear rate dependence of the viscosity, indicates that the polymer solutions are unentangled. (iv) The dynamic light scattering results at temperatures up to CP disclose the existence of initially an exponential decay (always diffusive) and a stretched exponential at longer times; this mode shows stronger q dependence than for a diffusive mode. The fast relaxation mode is associated with the diffusion of coils/contracted coils or small clusters, whereas the slow mode is attributed to interchain aggregation with the formation of aggregates or particles at higher concentration. Slightly above CP, the relaxation process is unimodal, and in this case, the high stickiness of the individual chain molecules evokes interchain association and the formation of large clusters. Because of the impoverishment of individual chains in the solution, the relaxation mode representing intrachain moieties disappears, and a single population of particles with a narrow size distribution is obtained.

The overall picture that emerges from this investigation, combining a variety of experimental techniques on an amphiphilic thermoresponsive polymer, is that in dilute solution a temperature increase leads to compression of individual polymer coils, whereas interchain aggregation dominates at higher concentration. At low temperature, increased polymer concentration induces collapse of chain molecules due to deteriorated thermodynamic conditions. At higher temperatures, the competition between increased stickiness and poorer thermodynamic conditions favors aggregation, and larger structures are formed. These species are likely to have a complex character, with the hydrophobic parts largely hidden from the solvent and the hydrophilic PEO side chains exposed to the aqueous surrounding.

Acknowledgment. B.N. and K.D.K. gratefully acknowledge support from the Norwegian Research Council trough a NANOMAT Project (158550/431). K.D.K. and C.G. thank the Marie Curie Industry Host Project (Contract G5TR-CT-2002-00089) for support.

References and Notes

(1) *Macromolecular Complexes in Chemistry and Biology*; Dubin, P., Bock, J., Davies, R. M., Schulz, D. N., Thies, C., Eds.; Springer-Verlag: Berlin, 1994.
(2) Muthukumar, M.; Ober, C. K.; Thomas, E. L. *Science* **1997**, *277*, 1225.
(3) Qiu, X.; Wu, C. *Macromolecules* **1997**, *30*, 7921.
(4) Förster, S.; Antonietti, M. *Adv. Mater.* **1998**, *10* 195.
(5) Kjøniksen, A.-L.; Nyström, B.; Lindman, B. *Macromolecules* **1998**, *31*, 1852.
(6) Wesslén, B. *Macromol. Symp.* **1998**, *130*, 403.
(7) Safford, M.; Polozova, A.; Winnik, F. M. *Macromolecules* **1998**, *31*, 7099.
(8) Heitz, C.; Prud'homme, R. K.; Kohn, J. *Macromolecules* **1999**, *32*, 6658.
(9) Zhu, P. W.; Napper, D. H. *Macromolecules* **1999**, *32*, 2068.
(10) Lowe, T. L.; Benhaddou, M.; Tenhu, H. *Macromol. Chem. Phys.* **1999**, *200*, 51.
(11) Lowe, T. L.; Tenhu, H.; Tylli, H. *J. Appl. Polym. Sci.* **1999**, *73*, 1031.
(12) Virtanen, J.; Tenhu, H. *J. Polym. Sci., Part A: Polym. Chem.* **2001**, *39*, 3716.
(13) Kjøniksen, A.-L.; Nyström, B.; Tenhu, H. *Colloids Surf. A Physicochem. Eng. Aspects* **2003**, *228*, 75.
(14) Laukkanen, A.; Valtola, L.; Winnik, F. M.; Tenhu, H. *Macromolecules* **2004**, *37*, 2268.
(15) Kronenthal, R. L.; Oser, Z.; Martin, E. *Polymer Science and Technology: Polymers in Medicine and Surgery*; Plenum Press: New York, 1975; Vol. 8.
(16) Hoffman, A. S.; Afrassiabi, A.; Dong, L. C. *J. Controlled Release* **1986**, *4*, 213.
(17) Shalaby, W. S.; et al. *Polymers of Biological and Biomedical Significance*; American Chemical Society: Washington, DC, 1994.
(18) Ottenbrite, R. M.; Huang, S. J.; Park, K. *Hydrogels and Biodegradable Polymers for Bioapplications*; American Chemical Society: Washington, DC, 1996.
(19) Mikheeva, L. M.; Grinberg, N. V.; Mashkevich, A. Y.; Grinberg, V. Y. *Macromolecules* **1997**, *30*, 2693.
(20) Vihola, H.; Laukkanen, A.; Valtola, L.; Tenhu, H.; Hirvonen, J. *Biomaterials,* in press.
(21) Taylor, L. D.; Cerankowski, L. D. *J. Polym. Sci., Polym. Chem. Ed.* **1975**, *13*, 2551.
(22) Moerkerke, R.; Koningsveld, R.; Berghmans, H.; Dušek, K.; Šolc, K. *Macromolecules* **1995**, *28*, 1103.
(23) Schäfer-Soenen, H.; Moerkerke, R.; Berghmans, H.; Koningsveld, R.; Dušek, K.; Šolc, K. *Macromolecules* **1997**, *30*, 410.
(24) Heskins, M.; Guillet, J. E. *J. Macromol. Sci., Chem.* **1968**, *A2*, 1441.
(25) Durand, A.; Hourdet, D. *Polymer* **2000**, *41*, 545.
(26) Lau, A. C. W.; Wu, C. *Macromolecules* **1999**, *32*, 581.
(27) Laukkanen, A.; Hietala, S.; Maunu, S. L.; Tenhu, H. *Macromolecules* **2000**, *33*, 8703.
(28) Meeussen, F.; Nies, E.; Berghmans, H.; Verbrugghe, S.; Goethals, E.; Du Prez, F. *Polymer* **2000**, *41*, 8597.
(29) Laukkanen, A.; Wiedmer, S. K.; Varjo, S.; Riekkola, M.-L.; Tenhu, H. *Colloid Polym. Sci.* **2002**, *280*, 65.
(30) Verbrugghe, S.; Laukkanen, A.; Aseyev, V.; Tenhu, H.; Winnik, F. M.; Du Prez, F. E. *Polymer* **2003**, *44*, 6807.
(31) Galaev, I. Y.; Mattiasson, B. *Trends Biotechnol.* **1999**, *17*, 335.
(32) Evans, D. F.; Wennerström, H. *The Colloidal Domain*, 2nd ed.; Wiley-VCH: New York, 1999.
(33) Ottewill, R. H.; Satgurunathan, R. *Colloid Polym. Sci.* **1995**, *273*, 379.
(34) Chen, M.-Q.; Serizawa, T.; Kishida, A.; Akashi, M. *J. Polym. Sci., Part A: Polym. Chem.* **1999**, *37*, 2155.
(35) Capek, I.; Murgašová, R.; Lath, D.; Lathová, E.; Juranicová, V.; Barton, B. *J. Polym. Sci., Part A: Polym. Chem.* **1999**, *37*, 3087.
(36) Liu, J.; Chew, C. H.; Gan, L. M. *J. Macromol. Sci., Pure Appl. Chem.* **1996**, *A33*, 337.
(37) Okhapkin, I. M.; Nasimova, I. R.; Makhaeva, E. E.; Khokhlov, A. R. *Macromolecules* **2003**, *36*, 8130.
(38) Yanul, N. A.; Kirsh, Y. E.; Verbrugghe, S.; Goethals, E. J.; Du Prez, F. E. *Macromol. Chem. Phys.* **2001**, *202*, 1700.
(39) Wignall, G. D.; Bates, F. S. *J. Appl. Crystallogr.* **1987**, *20*, 28.
(40) Siegert, A. J. F. Massachusetts Institute of Technology, Radiation Laboratory Report No. 465, 1943.
(41) Douglas, J. F.; Hubbard, J. B. *Macromolecules* **1991**, *24*, 3163.
(42) Wang, C. H.; Zhang, X. Q. *Macromolecules* **1993**, *26*, 707.
(43) Ngai, K. L. *Adv. Colloid Interface Sci.* **1996**, *64*, 1.
(44) Provencher, S. W. *Comput. Phys. Commun.* **1982**, *27*, 213, 229.
(45) Flory, P. J. *Principles of Polymer Chemistry*; Cornell University Press: Ithaca, NY, 1953.
(46) Malcolm, G. N.; Rowlinson, J. S. *Trans. Faraday Soc.* **1957**, *53*, 921.
(47) Baulin, V. A.; Halperin, A. *Macromolecules* **2002**, *35*, 6432.
(48) Karlström, G. *J. Phys. Chem.* **1985**, *89*, 4962.
(49) Matsuyama, A.; Tanaka, F. *Phys. Rev. Lett.* **1990**, *65*, 341.
(50) De Gennes, P.-G. *C. R. Acad. Sci., Ser. II* **1991**, *313*, 1117.
(51) Bekiranov, S.; Bruinsma, R.; Pincus, P. *Phys. Rev. E* **1997**, *55*, 577.
(52) Painter, P. C.; Berg, L. P.; Veytsman, B.; Coleman, M. M. *Macromolecules* **1997**, *30*, 7529.
(53) Semenov, A. N.; Rubinstein, M. *Macromolecules* **1998**, *31*, 1373.

(54) Borisov, O. V.; Halperin, A. *Macromolecules* **1999**, *32*, 5097.
(55) Beaucage, G. *J. Appl. Crystallogr.* **1995**, *28*, 717.
(56) Beaucage, G. *J. Appl. Crystallogr.* **1996**, *29*, 134.
(57) Stellbrink, J.; Willner, L.; Jucknishcke, O.; Richter, D.; Lindner, P.; Fetters, L. J.; Huang, J. S. *Macromolecules* **1998**, *31*, 4189.
(58) De Gennes, P.-G. *Scaling Concepts in Polymer Physics*; Cornell University Press: Ithaca, NY, 1979.
(59) Nyström, B.; Thuresson, K.; Lindman, B. *Langmuir* **1995**, *11*, 1994.
(60) Thuresson, K.; Lindman, B.; Nyström, B. *J. Phys. Chem. B* **1997**, *101*, 6450.
(61) Senff, H.; Richtering, W.; Norhausen, C.; Weiss, A.; Ballauff, M. *Langmuir* **1999**, *15*, 102.
(62) Chronakis, I. S.; Doublier, J.-L.; Piculell, L. *Int. J. Biol. Macromol.* **2000**, *28*, 1.
(63) Bromberg, L. *Langmuir* **1998**, *14*, 5806.
(64) Chassenieux, C.; Fundin, J.; Ducouret, G.; Iliopoulos, I. *J. Mol. Struct.* **2000**, *554*, 100.
(65) Lund, R.; Lauten, R. A.; Nyström, B.; Lindman, B. *Langmuir* **2001**, *17*, 8001.
(66) Colby, R. H.; Rubinstein, M.; Daoud, M. *J. Phys. II* **1994**, *4*, 1299.
(67) De Gennes, P.-G. *Macromolecules* **1976**, *9*, 587, 594.
(68) Colby, R. H.; Rubinstein, M. *Macromolecules* **1990**, *23*, 2753.
(69) Regalado, E. J.; Selb, J.; Candau, F. *Macromolecules* **1999**, *32*, 8580.
(70) Tsitsilianis, C.; Iliopoulos, I.; Ducouret, G. *Macromolecules* **2000**, *33*, 2936.
(71) Thuresson, K.; Nilsson, S.; Kjøniksen, A.-L.; Walderhaug, H.; Lindman, B.; Nyström, B. *J. Phys. Chem. B* **1999**, *103*, 1425.
(72) Vlassopoulos, D.; Fytas, G.; Pispas, S.; Hadjichristidis, N. *Physica B* **2001**, *296*, 184.
(73) Adam, M.; Delsanti, M. *Macromolecules* **1977**, *10*, 1229.
(74) Seery, T. A. P.; Shorter, J. A.; Amis, E. J. *Polymer* **1989**, *30*, 1197.
(75) Layec, Y.; Layec-Raphalen, M. N. *J. Phys., Lett.* **1983**, *44*, 121.
(76) Raspaud, E.; Lairez, D.; Adam, M.; Carton, J. P. *Macromolecules* **1994**, *27*, 2956.

MA048581Q